Universal Features of Metastable State Energies in Cellular Matter

Sangwoo Kim, Yiliang Wang, and Sascha Hilgenfeldt

Universal Features of Metastable State Energies in Cellular Matter

Sangwoo Kim,* Yiliang Wang,* and Sascha Hilgenfeldt

Mechanical Sciences and Engineering, University of Illinois, Urbana-Champaign, IL

(Dated: May 9, 2018)

Mechanical equilibrium states of Cellular Matter are overwhelmingly metastable and separated from each other by topology changes. Using theory and simulations, it is shown that for a wide class of energy functionals in 2D, including those describing tissue cell layers, local energy differences between neighboring metastable states as well as global energy differences between initial states and ground states are governed by simple, universal relations. Knowledge of instantaneous length of an edge undergoing a T1 transition is sufficient to predict local energy changes, while the initial edge length distribution yields a successful prediction for the global energy difference. An analytical understanding of the model parameters is provided.

In interacting many-particle systems, energy landscapes are complex and hard to analyze, in particular when disorder prevents symmetries. Considerable effort has focused on particle aggregates with short-range interactions (hard-core or soft) in the context of granular media [1–4], optimal packings [5–8], or the description of jammed states [9–12]. In *Cellular Matter*, on the other hand, the main energy contributions result from the shape and properties of the *interfaces* between deformable *domains* that fill available space (with a negligible continuous phase), making the interfaces surfaces of polygons (in two dimensions) or polyhedra (in three dimensions) [13, 14]. The exclusion of bulk energy contributions generally means that the areas (2D) or volumes (3D) of individual domains remain constant, while their shape and relative positioning is variable; the simplest physical example is a dry soap froth [15]. Cellular Matter also includes large classes of systems considered in the context of modeling biological tissues, with energy contributions from elasticity and cell-cell adhesion [16–18], bulk elasticity [19, 20], or viscous effects [21, 22].

Recent work has focused on low-energy states of Cellular Matter, which we will call "ground states", although the global lowest-energy state is in general unknown and may not be unique [23]. Ground states in this sense are found through a variety of protocols and annealing strategies, and their energies are typically insensitive to the method [23, 24]. Tissue-like 2D systems show a qualitative transition of the ground state: For low values of inter-domain adhesion energy (relative to elastic deformation penalties), the material ground state retains rigidity (finite resistance to external forces) [18], while for higher adhesion it becomes degenerate [25, 26] with individual domains minimizing their energy separately (the material becomes "floppy"). This "loss of rigidity transition" [19] occurs for static as well as for fluctuating systems, where it resembles a solid-fluid transition [19, 27].

The present work, by contrast, focuses on metastable states (local energy minima) significantly above the ground state energy. These are common in cellular systems in nature: If the energy barriers exceed thermal en-
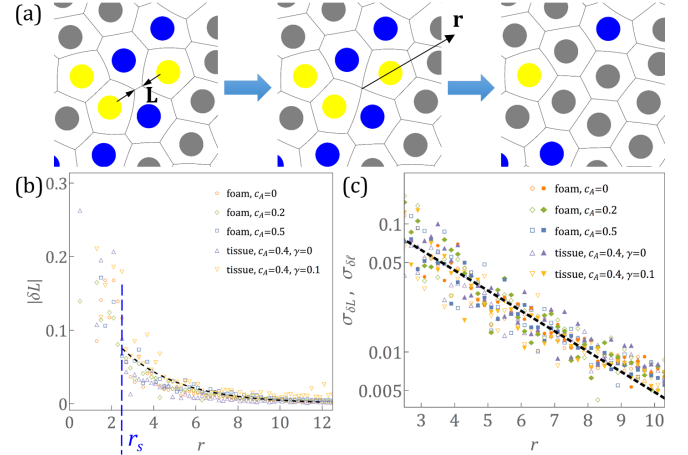

FIG. 1. (a) A T1 transition flipping an edge of initial length L, going through an unstable four-way intermediate configuration and ending up with altered topologies of adjacent cells. Colors represent polygonal edge number: 5 (yellow), 6 (grey), 7 (blue). (b) Binned plot of edge length change $|\delta L|$ as a function of distance r from the center of the T1 edge; r_s (vertical dotted line) is the distance beyond which the analytical model assumes stochastic length changes; (c) The standard deviations of absolute and relative edge length changes for $r > r_s$ decay as $\exp(-\kappa r)$ (black dashed line).

ergies, as expected for domains above colloidal size, a system needs induced stimuli to evolve towards the ground state. We show how limited information on the geometry of a generic rigid 2D cellular system quantitatively predicts the energy of the metastable states, governs individual topological transitions, and describes an efficient pathway of lowering energy towards a ground state.

Cellular matter domains (identified by index i) interact with nearest neighbors only, each contributing to a total energy $E = \sum_i E_i$. Restricting ourselves to 2D systems, the requirement of dominant interfacial energy means that we can generally write

$$E_i = \int_{P_i} u_{P,i}(s)ds = c_{0i}P_i + \frac{1}{2}c_{1i}P_i^2 + \dots, \quad (1)$$

expanding the general energy per length $u_{P,i}(s)$ in the perimeter lengths P_i. The shown truncation after the sec-

ond term is representative of the generic class of 2D tissue model studied in the recent literature [16, 18, 19, 25, 28]. For domains or cells of the same type, the coefficients are uniform (c_0, c_1).

Setting $c_1 = 0$ describes a 2D foam, identifying the interfacial tension with c_0 $(= 1$ without loss of generality). Including the second order term in P_i recovers the general case of "tissue" energy. By rearranging terms, we obtain the following two functionals,

$$E_f = \frac{1}{2\mathcal{L}_0}\sum_i P_i, \ E_t = \frac{1}{2\mathcal{L}_0}\sum_i \left(\frac{(P_i - P_{i,0})^2}{P_{i,0}} - \gamma P_i\right) \quad (2)$$

where all lengths are normalized by $\mathcal{L}_0$, the edge length of a regular hexagon of area A_{tot}/N for a system of N domains covering an area A_{tot}. In E_t, the first and the second terms can be interpreted as perimeter elasticity and adhesion energy, respectively [16, 18]. $P_{i,0}$ is the mechanical equilibrium perimeter of cell i in isolation, here chosen as the perimeter of a circle with the same area as domain i (other choices of $P_{i,0}$ merely rescale relevant energy differences [18]). The dimensionless adhesion strength γ is normalized by the perimeter elastic modulus. It was shown [17–19, 25] that loss of rigidity occurs when $\gamma > \gamma_c \approx 0.12$. Below this value, γ is a non-geometric determinant of system energy. We will show that energies can, nevertheless, be inferred from geometry alone.

Metastable states are separated from each other by *T1 topological transitions* [30], where a single edge of length L reorients (it "flips") to change topology of four neighboring cells (Fig. 1a). For rigid/solid states (foams or tissues with $\gamma < \gamma_c$), there are metastable states on both sides of the transition, while the intermediate state of four-way-connected edges is a local maximum (the energy barrier) [31].

We evaluate metastable states in Surface Evolver [32] (SE) with the quadratic or circular arc vertex models (i.e., edges between domains contain additional vertices and are generally not straight), on rectangles with periodic boundary conditions containing typically $N = 400$ or 900 domains. Initial patterns are Voronoi constructs from various point distributions. SE fixes domain areas to match a desired area distribution (polydispersity is quantified by its coefficient of variation c_A) and finds a local energy minimum with the given topology and energy functional. We analyze the metastable states after and before the T1. Geometrically, T1s are local events – the edge length changes $|\delta L|$ and their standard deviation $\sigma_{\delta L}$ decay exponentially with distance from the flipping edge. Figs. 1b,c identify a characteristic decay scale $\kappa^{-1} \approx 2.8$, in quantitative agreement with earlier findings [33].

This study focuses not on the energy barrier height between the states [28], but on the distribution of the energy differences ΔE between the system energies after
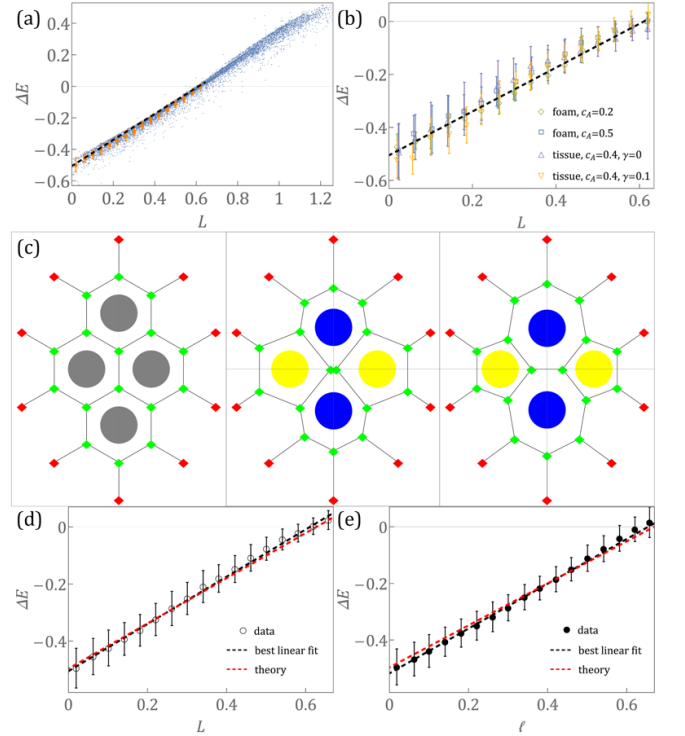

FIG. 2. (a) Energy change by T1 transition ΔE vs. initial edge length L in monodisperse foam samples (blue) with binned data for $\Delta E < 0$ (orange circles) and the overall linear relation (3) (dashed line); (b) the same in polydisperse foams and polydisperse tissue systems with different adhesion; (c) Simplified local configurations for analytical calculations: (left) monodisperse hexagonal pattern, (center) one quadruple defect with equal cell areas, (right) a quadruple defect with area polydispersity (at fixed total area). Vertex positions indicated in red are fixed, the others represent optimization variables. (d) Combined $\Delta E(L)$ data from all simulations, binned (circles) with best linear fit using α, L_c (black) and analytical linear relation using $\alpha_a, L_{c,a}$ (red); (e) like (d), for $\Delta E(\ell)$ data and correlations using β, ℓ_c and their analytical analogs $\beta_a, \ell_{c,a}$.

and before the T1. We find that the expectation value of ΔE has a strong linear correlation with the initial length L of the flipping edge,

$$\Delta E = \alpha\left(L - L_c\right). \quad (3)$$

As seen in Fig. 2a, the scatter around this linear relation is particularly small for energetically favorable T1s $(\Delta E < 0)$. For this range, data from $\gtrsim 30,000$ T1 transitions for systems of various polydispersities and various energy functionals were analyzed. It is a surprising fact that α and L_c are found to be system-independent and robust against protocol changes: (i) different methods of domain preparation – see the Supplemental Material – have no perceptible effect on (3) or on the scatter of the data; (ii) the order of T1s is irrelevant; (iii) widely different polydispersities result in the same values (Fig. 2b); (iv) even simulations using E_t are in quantitative agree-

ment with those using E_f: If the perimeter lengths of the tissue in mechanical equilibrium are P_i^*, computing $E_f^* = \frac{1}{2\mathcal{L}_0}\sum_i P_i^*$ yields an equivalent foam energy whose correlation with L is quantitatively the same (Fig. 2b), even though the energetics of the T1 processes that yield the configurations are quite different, and the configurations are not metastable states under E_f. The linear correlation (3) remains unchanged for all "tense" tissues ($\gamma < \gamma_c$). Beyond γ_c, the system loses rigidity and all ΔE are trivially zero. Very recent work on three-dimensional epithelial sheets [27] likewise finds a linear relation between flipping-face area and energy differences in agreement with (3).

An average over all data is described well by (3) with a *universal* critical edge length $L_c \approx 0.611$ and a *universal* slope $\alpha \approx 0.827$. Beyond empirical data, we can obtain analytical approximations to α and L_c from the simple elementary T1 transition between a honeycomb pattern and a quadruple defect (two neighboring dislocations, Fig. 2c). Changing the areas of the pentagons and heptagons generates elementary polydisperse configurations. All vertices not belonging to cells participating in the T1 are fixed at their honeycomb positions (red in Fig. 2c). Minimizing $E_{f,t}$ with respect to the remaining degrees of freedom yields analytical metastable state geometries as solutions to a system of algebraic equations (see Supplemental Material). A linear fit to the resulting $\Delta E(L)$ values obtains $\alpha_a \approx 0.791$ and $L_{c,a} \approx 0.627$, in very good agreement with data (Fig. 2d).

Now we use this information about energetic effects of (spatially local) T1s to infer the *global* energy of a given metastable state, not only for purposes of easy general diagnostics, but in order to assess whether metastability interferes with the ability to detect the loss-of-rigidity transition mentioned above. Both simulations and analytical computations are used. The simulations should reflect processes of mechanical excitation overcoming energy barriers, e.g. by shearing foams [34, 35], agitating emulsions [36, 37] or by cell mobility in tissues [38], so that the system energy approaches a ground state through successive T1s. Eq. (3) suggests flipping short edges ($L < L_c$) will selectively lower the system energy. However, simulations may miss energetically favorable edge flips if these edges are surrounded by large-area cells (they are relatively short, but absolutely longer than L_c). Therefore, we shall focus on *relative* edge length ℓ,

$$\ell = L/\min(L_{0i}, L_{0j}),\qquad(4)$$

where $L_{0i} = 2^{1/2}3^{-3/4}A_i^{1/2}$ is the edge length of a regular hexagon of area A_i, and the domains i, j share the edge. As Fig. 2e shows, $\Delta E(\ell)$ is still a linear function,

$$\Delta E = \beta\left(\ell - \ell_c\right),\qquad(5)$$

and can still be described with system-independent parameters $\ell_c \approx 0.654$ and $\beta \approx 0.791$ (see Supplemental
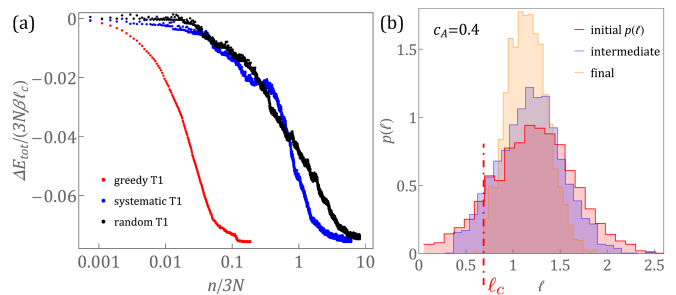

FIG. 3. (a) Decrease of energy with the number of T1 transitions for three different algorithms. The "greedy" algorithm always flips the current shortest edge and yields a very good approximation to the ground state energy in a small number of steps. (b) Evolution of the relative edge length probability distribution $p_n(\ell)$ for a polydisperse ($c_A = 0.4$) foam sample of $N = 900$, showing distributions at $n = 0$ ($p(\ell)$), $n = 88$, and $n = n_{\text{fin}} = 324$.

Material for data). These parameters can be understood by analyzing the extreme cases: Near the ground state, the domain shapes do not deviate much from regular polygons, for which the ratio of perimeter to $A^{1/2}$ is essentially constant [39]. An average polygon undergoing a T1 with $L \approx L_c$ then has a shorter perimeter by the factor $(5 + L_c)/6$; with (4) this leads to the estimate $\ell_{c,a} = 6L_c/(5 + L_c) \approx 0.654$. Conversely, any T1 with $\ell \to 0$ must have the same result as $L \to 0$, so that $\alpha L_c = \beta \ell_c$, resulting in $\beta_a \approx 0.772$. The analytical estimate again proves very accurate (Fig. 2e).

Our SE simulations establish metastable states after every T1 of a selected edge. Figure 3a compares the energy reduction $\Delta E_{\text{tot}}(n) = E(n) - E(0)$ after n T1s using different selection strategies: systematic cycling through a complete list of edges, random selection, and the "greedy" algorithm suggested by (5), which always flips the edge with the shortest current ℓ. All algorithms reverse T1s with $\Delta E > 0$, and try a different edge next; they all asymptote to very similar energies (supporting the notion of a well-defined ground state energy), but the greedy algorithm needs much less computational effort (and its final energy is slightly lower). These findings are independent of polydispersity or energy functional.

Analytically, a total energy drop as in Fig. 3a can be predicted under the assumption that the effects of the (spatially localized) T1s are independent. Then, $E_{tot}(n)$ can be inferred from the initial probability distribution $p(\ell)$ only – precisely those edges with $\ell < \ell_c$ should flip. In Fig. 3b, a typical development of $p(\ell)$ with n in simulations is shown – indeed, the probability weight below ℓ_c becomes negligible towards the end.

Then, an edge of length ℓ flips after $n(\ell)$ T1s, such that

$$n(\ell) = 3N\int_0^\ell p(\ell')d\ell',\qquad(6)$$

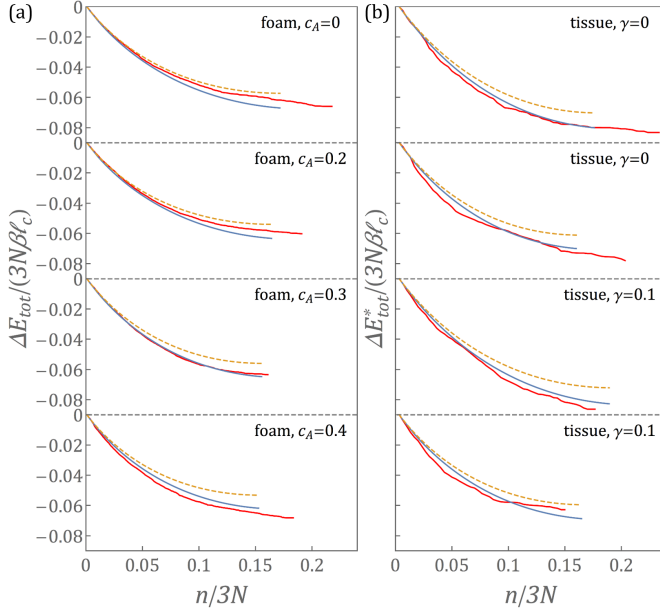where $3N$ is the total number of edges, and the predicted

FIG. 4. Energy decrease with T1 number n comparing the simulation results (red; greedy algorithm) with theoretical predictions from (8) (orange, dashed) and the refined theory (9) (blue, solid). (a) Foams of different polydispersity, using E_f; (b) Tissues (E_f^*, $c_A = 0.4$) with $\gamma = 0$ and $\gamma = 0.1$.

final number of T1s is $n_{\text{fin}} = n(\ell_c)$. It follows that

$$\Delta E_{tot}(n) = \int_0^{\ell(n)} 3N \Delta E(\ell) p(\ell) d\ell \,, \qquad (7)$$

where $\ell(n)$ is given by inverting (6). Taking into account (5) and using integration by parts, it is easy to show that

$$\frac{\Delta E_{tot}(n)}{3N\beta\ell_c} = \frac{\ell(n) - \ell_c}{\ell_c} P(\ell(n)) - \frac{1}{\ell_c} \int_0^{\ell(n)} P(\ell) d\ell \,, \quad (8)$$

with $P(\ell) \equiv \int_0^\ell p(\ell') d\ell'$. Eq. (8) gives the predicted energy decrease as a fraction of a hypothetical maximum; note that $-\beta\ell_c = \Delta E(0)$ according to (5).

The prediction (8) only needs the initial distribution $p(\ell)$ for $\ell < \ell_c$; any integrable fit to $p(\ell)$ yields an explicit analytical expression for ΔE_{tot}. Figure 4 compares greedy simulation results of different foams and tissues (only energy-lowering steps are accepted) with (8); for tissue systems, equivalent foam energies E_f^* are again used. The agreement is good, but $|\Delta E_{tot}|$ is systematically underestimated by typically $5 - 15\%$.

This bias can be eliminated by modeling the shape changes in $p_n(\ell)$ shown in Fig. 3b; these come about because T1s induce exponentially decaying fluctuations in the absolute or relative lengths of edges beyond a characteristic distance r_s (cf. Fig. 1b,c). This stochastic fluctuation of width σ_ℓ acts as a convolution on $p(\ell)$, increasing its width and lowering the value of $\ell(n)$ to $\ell(n) - \Delta\ell$, so that the currently shortest edges become slightly shorter and their T1 lowers the energy slightly

more. The system-independence of the features seen in Fig. 1c and Fig. 2e allows for an analytical computation for this convolution in the limit of Gaussian distributions, from which $\Delta\ell \approx 0.037$ follows. The details are found in the Supplemental Material.

Accordingly, we modify (8) to

$$\frac{\Delta E_{tot}(n)}{3N\beta\ell_c} = \frac{\ell_{\text{eff}}(n) - \ell_c}{\ell_c} P(\ell(n)) - \frac{1}{\ell_c} \int_0^{\ell(n)} P(\ell) d\ell \,, \quad (9)$$

with $\ell_{\text{eff}} = \max(\ell - \Delta\ell, 0)$, to avoid negative edge lengths. The systematic error in the comparisons to simulation results is largely eliminated (see Fig. 4), though a statistical error of a few % remains (see Supplemental Material). The predicted $|\Delta E_{tot}|$ is still obtained from the initial distribution only, and thus the asymptotic ground state energy is accurately predicted from just a snapshot of an initial metastable state. We stress that the simulations employ a variety of strategies for annealing to the ground state [40], which can lead to a larger empirical n_{fin}, but nevertheless this "single-shot" prediction of ΔE_{tot} is in good agreement. Also note that tissue samples with $\gamma = 0.1$ are much closer to the critical γ_c than those with $\gamma = 0$, but the quality of the prediction is unchanged.

We have demonstrated that the geometry of 2D metastable states quantitatively determines their energy both locally and globally, beyond the trivial summing of edge lengths to obtain a foam energy: locally, the ΔE of a T1 is predicted by its edge length. Globally, T1 energies integrate to approximate the metastable state energy above the ground state ΔE_{tot}. Energy-lowering T1 transitions are almost exclusively confined to edges with relative length $\ell < \ell_c$, and the critical value is universal across polydispersities and energy functional forms. Only these edges "store" the structural energy above the ground state, and they are relatively few (we did not find metastable states with $P(\ell_c) > 0.18$). Apart from the foam and tissue models discussed here, we have conducted less extensive simulations with energy functionals including area elasticity, with altered boundary conditions, and even with spring-like interactions, without changes to the reported relations. The remarkable simplicity and generality of these findings is reminiscent of the classification of rigid and floppy ground states by the purely geometric shape index $\bar{p} = \sum_i P_i/A_i^{1/2}/N$ of the domains, independent of energy functionals [18, 19, 41]. Likewise, we rationalize the universal nature of the relations by the strong geometric constraints imposed by a space-filling 2D structure with rigid domain boundaries, making all possible T1 energy changes perturbative. Beyond the loss of rigidity transition, domains acquire different geometric degrees of freedom, and the relations cease to be valid. Importantly, however, our results show that metastable states of rigid/solid systems can have values of $\bar{p}$ (i.e., equivalent foam energies) significantly *larger*

than the critical $\bar{p}_c$ for loss of rigidity *in the ground state.* While there are other indicators of floppy/fluid systems, this illustrates that the diagnostic meaning of $\bar{p}$ depends on whether the system is close to the ground state.

According to our results, a simple snapshot of any metastable 2D sample (a tissue, an emulsion, a polycrystal) in a rigid/solid state suffices to classify it in terms of its distance from the type of ground state analyzed in previous work [19, 25]. Short edges are weak spots favoring T1 transitions, and a heterogeneous spatial distribution indicates mechanically weak regions. The diagnostics of material properties and their spatial distribution (in industrial applications) or the occurrence and distribution of pathological changes (in biological tissues) is aided by these findings. The geometric information used here can be further combined with topological statistics [29, 34, 42], which is the subject of ongoing work [43].

---

* These two authors contributed equally.

[1] C. h. Liu, S. R. Nagel, D. A. Schecter, S. N. Coppersmith, S. Majumdar, O. Narayan, and T. A. Witten, Science **269**, 513 (1995).

[2] H. M. Jaeger, S. R. Nagel, and R. P. Behringer, Rev. Mod. Phys. **68**, 1259 (1996).

[3] D. Lohse, R. Rauhé, R. Bergmann, and D. van der Meer, Nature **432**, 689 EP (2004).

[4] T. S. Majmudar and R. P. Behringer, Nature **435**, 1079 EP (2005).

[5] A. Donev, I. Cisse, D. Sachs, E. A. Variano, F. H. Stillinger, R. Connelly, S. Torquato, and P. M. Chaikin, Science **303**, 990 (2004).

[6] W. Man, A. Donev, F. H. Stillinger, M. T. Sullivan, W. B. Russel, D. Heeger, S. Inati, S. Torquato, and P. M. Chaikin, Phys. Rev. Lett. **94**, 198001 (2005).

[7] T. Aste and D. Weaire, *The Pursuit of Perfect Packing* (IOP, London, 2000).

[8] S. Torquato, T. M. Truskett, and P. G. Debenedetti, Phys. Rev. Lett. **84**, 2064 (2000).

[9] S. Torquato and F. H. Stillinger, Rev. Mod. Phys. **82**, 2633 (2010).

[10] S. Atkinson, F. H. Stillinger, and S. Torquato, Proceedings of the National Academy of Sciences **111**, 18436 (2014).

[11] A. J. Liu and S. R. Nagel, Annual Review of Condensed Matter Physics **1**, 347 (2010).

[12] C. E. Zachary, Y. Jiao, and S. Torquato, Phys. Rev. Lett. **106**, 178001 (2011).

[13] S. Hilgenfeldt, A. M. Kraynik, S. A. Koehler, and H. A. Stone, Phys. Rev. Lett. **86**, 2685 (2001).

[14] S. Hilgenfeldt, A. M. Kraynik, D. A. Reinelt, and J. M. Sullivan, EPL (Europhysics Letters) **67**, 484 (2004).

[15] D. Weaire and S. Hutzler, *The Physics of Foams* (Oxford University Press, Oxford, 2000).

[16] S. Hilgenfeldt, S. Erisken, and R. W. Carthew, Proceedings of the National Academy of Sciences **105**, 907 (2008).

[17] M. L. Manning, R. A. Foty, M. S. Steinberg, and E.-M. Schoetz, Proceedings of the National Academy of Sciences **107**, 12517 (2010).

[18] S. Kim and S. Hilgenfeldt, Soft Matter **11**, 7270 (2015).

[19] D. Bi, J. H. Lopez, J. M. Schwarz, and M. L. Manning, Nat Phys **11**, 1074 (2015).

[20] A. Fletcher, M. Osterfield, R. Baker, and S. Shvartsman, Biophysical Journal **106**, 2291 (2014).

[21] G. W. Brodland and J. H. Veldhuis, Journal of Biomechanics **35**, 673 (2002).

[22] G. W. Brodland, D. I.-L. Chen, and J. H. Veldhuis, International Journal of Plasticity **22**, 965 (2006).

[23] G. Zhang, F. Stillinger, and S. Torquato, Physical Review E **96**, 042146 (2017).

[24] M. Alava, P. Duxbury, C. Moukarzel, and H. Rieger, Phase Transitions and Critical Phenomena **18**, 143 (2001).

[25] D. Staple, R. Farhadifar, J. C. Röper, B. Aigouy, S. Eaton, and F. Jülicher, The European Physical Journal E: Soft Matter and Biological Physics **33**, 117 (2010).

[26] R. Farhadifar, J.-C. Röper, B. Aigouy, S. Eaton, and F. Jülicher, Current Biology **17**, 2095 (2007).

[27] M. Krajnc, S. Dasgupta, P. Ziherl, and J. Prost, (2017), *Fluidization of sheet-like tissues by active cell rearrangements*, preprint.

[28] D. Bi, J. H. Lopez, J. M. Schwarz, and M. L. Manning, Soft Matter **10**, 1885 (2014).

[29] S. Kim, J. J. Cassidy, B. Yang, R. W. Carthew, and S. Hilgenfeldt, Biophysical Journal **111**, 2735 (2016).

[30] D. Weaire and N. Rivier, Contemporary Physics **25**, 59 (1984).

[31] J. E. Taylor, Annals of Mathematics , 489 (1976).

[32] K. Brakke, Experimental Mathematics **1**, 141 (1992).

[33] S. Cox, F. Graner, and M. F. Vaz, Soft Matter **4**, 1871 (2008).

[34] C. Quilliet, S. A. Talebi, D. Rabaud, S. C. J. Käfer, and F. Graner, Philosophical Magazine Letters **88**, 651 (2008).

[35] A. Wyn, I. Davies, and S. Cox, The European Physical Journal E: Soft Matter and Biological Physics **26**, 81 (2008).

[36] D. Chen, K. W. Desmond, and E. R. Weeks, Soft Matter **8**, 10486 (2012).

[37] Y. Gai, C. M. Leong, W. Cai, and S. K. Tang, Proceedings of the National Academy of Sciences **113**, 12082 (2016).

[38] C. Collinet, M. Rauzi, P.-F. Lenne, and T. Lecuit, Nature cell biology **17**, 1247 (2015).

[39] F. Graner, Y. Jiang, E. Janiaud, and C. Flament, Physical Review E **63**, 011402 (2000).

[40] See the Supplemental Material for details, as well as H. X. Zhu, S. M. Thorpe, and A. H. Windle, Philosophical Magazine A **81**, 2765 (2001); S. Lloyd, IEEE Trans. Inf. Theor. **28**, 129 (2006).

[41] J.-A. Park, J. H. Kim, D. Bi, J. A. Mitchel, N. T. Qazvini, K. Tantisira, C. Y. Park, M. McGill, S.-H. Kim, B. Gweon, *et al.*, Nature materials **14**, 1040 (2015).

[42] M. P. Miklius and S. Hilgenfeldt, Phys. Rev. Lett. **108**, 015502 (2012).

[43] S. Kim and S. Hilgenfeldt, (2018), *Statistical Measures predict Inherent Structure in Two-Dimensional Cellular Matter Energy* (preprint).